Electric Power Systems Research 144 (2017) 13–22

Contents lists available at ScienceDirect

Electric Power Systems Research

journal homepage: www.elsevier.com/locate/epsr

Fault-tolerant location of transient voltage disturbance source for DG integrated smart grid

Guoqing Weng[a], Feiteng Huang[a], Yufei Tang[b], Jun Yan[c], Yurong Nan[a], Haibo He[c,*]

[a] College of Information Engineering, Zhejiang University of Technology, Hangzhou 310023, China
[b] Department of Computer & Electrical Engineering and Computer Science, Florida Atlantic University, Boca Raton, FL 33431, USA
[c] Department of Electrical, Computer, and Biomedical Engineering, University of Rhode Island, Kingston, RI 02881, USA

ARTICLE INFO

Article history:
Received 8 June 2016
Received in revised form
13 September 2016
Accepted 29 October 2016

Keywords:
Transient voltage disturbance source (TVDS)
Automatic location
Distributed generation (DG)
Direction-judgment
Fault tolerance
Improved particle swarm optimization (IPSO)

ABSTRACT

In this paper, a new fault-tolerant approach based on improved particle swarm optimization (IPSO) is proposed to automatically locate the transient voltage disturbance source (TVDS) for smart grid with distributed generation (DG) integration. We first analyze the influence of the DG integration on the TVDS direction-judgments. Two new credibility indexes, the monitoring-credibility and the partial-credibility, are defined to measure the reliability of direction-judgment result at each power quality monitor (PQM) with consideration of multiple factors, including DG integration, disturbance intensity and fluctuation characteristic. By using these credibility indexes and a newly defined search space, a heuristic searching approach, called IPSO, is then proposed to obtain the optimal solution of the TVDS location. Simulation study is carried out on the IEEE 34 node test feeder, and the results demonstrate that the proposed approach has significantly improved fault-tolerant capability with satisfatory convergence speed.

1. Introduction

It is widely recognized that power quality (PQ) will increasingly play an important role in providing economic, secure and stable energy in modern power systems [1]. In intelligent diagnosis of PQ disturbance events, in addition to the detection and classification problem [2–4], another important task is to locate the PQ disturbance sources. Statistically, transient voltage disturbance events (e.g. voltage sag and voltage swell) account for the highest number of occurrence compared to other PQ events [5]. Usually, these transient voltage disturbance events are caused by short faults, switching of capacitors, energization of large induction motors, lightning striking, etc. The accurate location of the transient voltage disturbance source (TVDS) can help provide accurate identification of the disturbance source, and facilitate suitable mitigation measures to reduce the economic loss.

In general, there are two distinctive categories of research methodologies for the automatic location of the TVDS. The first is based on pattern recognition and artificial intelligence [6–9] using a small quantity of power quality monitors (PQMs) for location, but these methods require complicated training processes for different types of TVDS and are sensitive to the grid's size and structural changes. With growing installation of networked power quality monitoring system (NPQMS) in modern smart grid [10], another category is based on the graph theory and matrix algorithm [11–13]. The existing matrix methods commonly consist of two major steps. The first step is the direction-judgment at each PQM to identify the relative direction of the TVDS to each PQM. In the literature, the disturbance energy (DE) algorithm was first proposed for the voltage-sag events [14]. Following this work, some improved algorithms have been presented for the direction-judgment of TVDS [15,16]. After the direction information is collected, the second step is the automatic location of the TVDS at the monitoring center. With the development of optimal placement techniques [17] and state estimation theory [18,19], the PQ information of nodes not equipped with actual PQMs could also be observed by viewing these nodes as virtual PQMs [13]. Compared with the first category, the latter has many advantages, including applicability to different types of TVDS, little influence from the grid's size and structure, and no need for training.

However, we notice that most of the existing matrix methods lack fault-tolerant capability, as the accuracy of the location result

* Corresponding author.
E-mail address: he@ele.uri.edu (H. He).

http://dx.doi.org/10.1016/j.epsr.2016.10.063
0378-7796/

of the TVDS is largely dependent on the absolute reliability of the direction-judgment at each PQM in the NPQMS. Even worse, it is difficult to guarantee the accuracy of all the direction-judgment results in a practical distribution grid. Particularly, distributed generation (DG) connection to the smart grid for utilization of the renewable energy is gradually increasing, which will have noticeable impacts on the power quality [20] and bring great challenges to the existing methods to locate the TVDS [21]. Moreover, many factors, such as the intensity and fluctuation characteristic of the PQ disturbance signals, the external interferences, state estimation, etc., can affect the reliability, or credibility, of the direction-judgment result. As an attempt, the disturbance measure (DM) was defined to describe the reliability of the direction-judgment result [22] with consideration of the disturbance intensity. Nonetheless, with more factors influencing the judgment result, it still requires more efforts to develop methods with high fault-tolerant capability.

In this paper, we first analyze the influence of DG integration and other factors to the reliability of the direction-judgment result at each PQM in the NPQMS. Then, a novel fault-tolerant approach based on an improved particle swarm optimization (IPSO) is proposed to locate the TVDS for DG integrated smart distribution grid. The main contributions of this paper are summarized as follows:

1. Two important influence rules of DG integration based on the detailed analysis with a scalable grid model are proposed. The rules show the scenarios that may lead to mistakes or reliability weakening in direction-judgment at the PQMs, which is the basis to solve the problem of TVDS location caused by DG integration.
2. Two new credibility indexes called monitoring-credibility and partial-credibility are defined. The first index can denote quantitatively not only the direction-judgment result of TVDS at each PQM but also the reliability of the result considering multiple influence factors. The later one can verify whether the direction misjudgment takes place at each PQM according the first influence rule.
3. A novel fault-tolerant approach, based on an IPSO algorithm is proposed to automatically locate the TVDS for DG integrated smart grid. In the IPSO, the evaluation function has been carefully constructed to synthetically utilize the credibility indexes, and the search space has been reduced greatly. Simulation results demonstrate that the proposed approach has significantly improved fault-tolerant capability, fast convergence speed and good applicability for various types of TVDS.

The rest of this paper is organized as follows. Section 2 describes the limitations of existing methods. Section 3 presents the influence rules of DG integration on direction-judgments. Section 4 constructs the credibility indexes based on comprehensive factors. Section 5 describes the IPSO model with the key steps to obtain the optimal solution. Section 6 carries out the simulations and analyzes the results, and Section 7 draws the conclusions.

2. Limitation of existing matrix-based methods

In the existing methods for locating the TVDS based on the matrix algorithm [11–13], a coverage-matrix $S^{cov}_{l\times m}$ is first generated to represent the relative positions between each line and each PQM in the grid, where l and m are the total numbers of lines and PQMs. Then, the direction-matrix $D^{dir}_{m\times 1}$, representing the relative positions between the TVDS and each PQM, is obtained based on the direction-judgment algorithm when PQ event happens. The elements of the two matrixes $S^{cov}_{l\times m}$ and $D^{dir}_{m\times 1}$ are defined as follows:

$$s_{ji}, d_i = \begin{cases} +1, & if \quad L_j \text{ or } TVDS \text{ is in down-area of PQM}_i \\ -1, & if \quad L_j \text{ or } TVDS \text{ is in up-area of PQM}_i \end{cases} \quad (1)$$

In the DE and its improved algorithms [14,16], the final polarity of the DE signal determines the relative position (upstream or downstream) between the TVDS and PQM. The result-matrix $R_{l\times 1}$ can be calculated by $R_{l\times 1} = S^{cov}_{l\times m} \cdot D^{dir}_{m\times 1}$. If the maximum of R, e.g. $r_j = max(r_1, r_2, \ldots, r_l)$ equals to m, then the line L_j corresponding to r_j is determined as the TVDS. If any error exists in the direction-judgments, then the location result of the TVDS would be incorrect [22,23]. Although it is fairly clear to use the signed binary integers (i.e. +1 or −1) to denote the relative positions of the TVDS with respect each PQM, this requirement of absolute reliability of all the direction-judgment results in $D^{dir}_{m\times 1}$ leads to a lack of fault-tolerant capability. In general, the factors that will cause misjudgment could be summarized as follows.

(1) DG integration: The traditional radial network with single power supply is evolved into multi-source distribution system, which will have a significant variation of the power flow distribution [20,21]. In general, the DG integration affects the intensity of the transient voltage disturbance signal, and at worst, may cause the direction misjudgment [24]. The detailed influences of the DG integration will be discussed in the next section.

(2) Disturbance intensity: Due to line loss and bypass flow, the intensity of the transient voltage disturbance signals detected at monitors far away from the TVDS are relatively weak [22,23]. Given the same condition of external interferences, such as noise signals, errors caused by measurement, transmission or state estimation, the direction misjudgment is more likely to happen with weak disturbance signal.

(3) Fluctuation characteristic: The polarity of the disturbance power may change frequently due to the energy-storage, reactive load, etc. These changes will further induce intensive fluctuation of the DE signal, resulting in uncertain monotonicity or even reversed final polarity of the DE signal [14]. In either case, the direction-judgment result is more likely to be incorrect.

3. Influence of DG integration

3.1. Scalable model and denotations

To analyze the influence of DG integration to the entire grid when a transient voltage disturbance event occurs, we designed a scalable grid model with one DG interconnection, whose topology is shown in Fig. 1. The partial networks $\{N_a, N_b, N_c, N_n\}$ in this figure represent the equivalents of sub-networks with a tree structure, enabling the scalable model to be expanded into most of the distribution systems with radial structure.

Similar to the area-dividing method in [12], the entire scalable model can be divided into up-area and down-area based on the

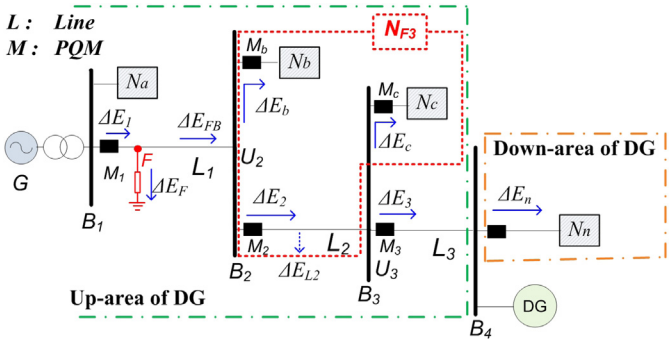

Fig. 1. Scalable grid model and up/down area of DG.

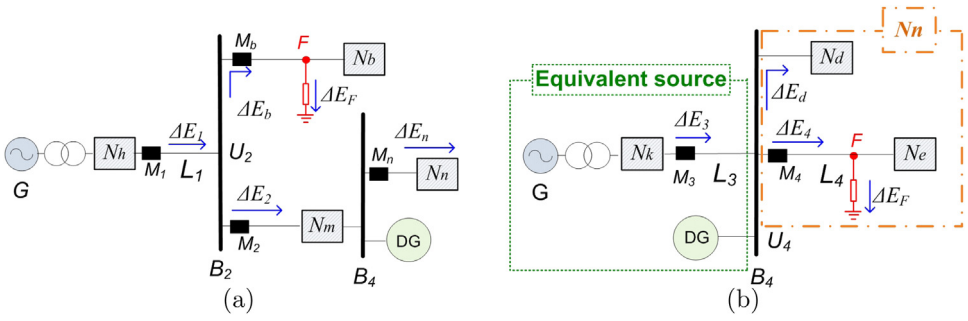

Fig. 2. Simplified model with F is not on $Link_{(G\_D\ G)}$: (a) F on the branch of $Link_{(G\_D\ G)}$ in the up-area of DG; (b) F in the down-area of DG.

DG location. The positive directions of the energy flows are defined and marked by solid blue arrows. Considering both the actual and the virtual PQMs, the PQ information at each line is observable. The important denotations for the discussion in this section are defined as follows: F is the location of the TVDS; $Link_{(G\_D\ G)}$ is the link between G and DG; $Link_{(F\_D\ G)}$ is the link between F and DG; $Bus_{(F\_D\ G)}$ is the bus connected to F at the side of DG; N_{Fi} is the current-dividing network that includes all the partial networks and the lines between $Bus_{(F\_D\ G)}$ and M_i; ΔE_i it the DE value that detected at M_i; ΔE_F is the DE value absorbed by the TVDS; ΔE_{FB} is the DE value that transmits from F to $Bus_{(F\_D\ G)}$; ΔE_{Fi} is the DE value absorbed by N_{Fi}; ΔU_F is the voltage variation at F; ΔU_{Bn} is the voltage variation at bus B_n; v' is the value of an unspecified state variable during the transient voltage disturbance event with DG not connected.

3.2. Rules of influence of DG integration

We consider two cases to understand the influence of DG integration on TVDS location in a voltage sag event. In general, the analysis procedure shown here could also be applied to other transient voltage disturbances (i.e. voltage swell caused by energy injection) just by reserving the polarity of the parameters.

3.2.1. F *is on* $\text{Link}_{(G\_DG)}$

As shown in Fig. 1, we assume that a DG is connected to the grid at B_4 when a voltage-sag event occurs at L_1. $Link_{(G\_DG)}$ and $Link_{(F\_DG)}$ are $\{G\_L_1\_L_2\_L_3\_DG\}$ and $\{F\_L_2\_L_3\_DG\}$ in this case, respectively. Because voltage-sag is an energy-absorbing disturbance [14,16], we have $\Delta E_F > 0$, $\Delta U_F < 0$, and $\Delta U_{B2} < 0$. The polarity of power flow at L_1 could be positive or negative because of the DG integration [21,24]. In either case, $\Delta E_b < 0$ and $\Delta E_{FB} < 0$. Based on the energy conservation law, we can obtain $\Delta E_2 = \Delta E_{FB} - \Delta E_b$ at bus B_2.

Considering N_b is actually N_{F2}, we have $\Delta E_2 = \Delta E_{FB} - \Delta E_{F2}$. Therefore, there are three possible direction-judgment results at M_2 as shown in Eq. (2) as follows:

$$\Delta E_2 = \begin{cases} > 0, & if \quad |\Delta E_{F2}| > |\Delta E_{FB}| \\ = 0, & if \quad |\Delta E_{F2}| = |\Delta E_{FB}| \\ < 0, & if \quad |\Delta E_{F2}| < |\Delta E_{FB}| \end{cases} \tag{2}$$

Similar analysis can be applied to the bus B_3. The current-dividing network of M_3 is N_{F3}, and three possible direction-judgment results can also be obtained at M_3. The direction-judgment results at M_2 and M_3 will be incorrect when $|\Delta E_{F2}| > |\Delta E_{FB}|$ and $|\Delta E_{F3}| > |\Delta E_{FB}|$, respectively. These inequality conditions are more likely to occur with the increase of power loads of the current-dividing. In this case, we propose the first rule of influence of DG integration:

First rule of influence: The direction-judgment result at PQM_i is incorrect and should be reversed when F is on $Link_{(G\_DG)}$, PQM_i is on $Link_{(F\_DG)}$, and $|\Delta E_{Fi}| > |\Delta E_{FB}|$.

In addition, the integrated DG at B_4 will contribute to the voltage stability, so we have $\Delta U_{B4} < 0$ and $|\Delta U_{B4}| < |\Delta U'_{B4}|$. The changes of the DE value in the down-area of the DG can be deduced as:

$$\Delta E'_n < \Delta E_n < 0 \tag{3}$$

3.2.2. F *is not on* $\text{Link}_{(G\_D\ G)}$

In this case, there are two different scenarios. The first scenario is that F locates on the branch of $Link_{(G\_D\ G)}$ in the up-area of DG, and then Fig. 1 can be simplified as Fig. 2(a). The second scenario is that F locates in the down-area of the DG, as shown in Fig. 2(b). In the second scenario, the partial network N_n is expanded to two sub-networks (N_d and N_e), and G and DG can be regarded as one equivalent source.

In Fig. 2(a), considering the effect of voltage stability with the DG integration, when the voltage-sag occurs we have $\Delta E_F > 0$, $\Delta U_{B2} < 0$, $\Delta U_{B4} < 0$, $|\Delta U_{B2}| < |\Delta U'_{B2}|$ and $|\Delta U_{B4}| < |\Delta U'_{B4}|$. Similarly, we could have $\Delta U_{B4} < 0$ and $|\Delta U_{B4}| < |\Delta U'_{B4}|$ in Fig. 2(b). The variations of the DE values at the PQMs in these two scenarios can be deduced as:

$$\begin{cases} 0 < \Delta E_1 < \Delta E'_1 \\ \Delta E'_2 < \Delta E_2 < 0 \\ \Delta E'_n < \Delta E_n < 0 \\ 0 < \Delta E'_b < \Delta E_b \end{cases} \quad and \quad \begin{cases} 0 < \Delta E_3 < \Delta E'_3 \\ \Delta E'_d < \Delta E_d < 0 \\ 0 < \Delta E'_4 < \Delta E_4 \end{cases} \tag{4}$$

Eq. (4) suggests that, if F is not on $Link_{(G\_DG)}$, the direction-judgment result at each PQM will still be correct. However, the disturbance intensity at all branches except for the F branch is weakened due to DG integration. According to Eqs. (3) and (4), we propose the second rule of influence of the DG integration as follows:

Second rule of influence: If PQM_i is not on $Link_{(F\_DG)}$, the disturbance intensity at PQM_i is weakened by the DG integration, but the direction-judgment is not affected.

4. Credibility of direction-judgment

4.1. Monitoring-credibility

To denote the effect of the factors to the reliability of the direction-judgment results, a new index c_i named monitoring-credibility is defined. We will first introduce three coefficients with respect to the polarity, disturbance intensity, and fluctuation characteristic. The following coefficients are valid to both voltage sag and voltage swell.

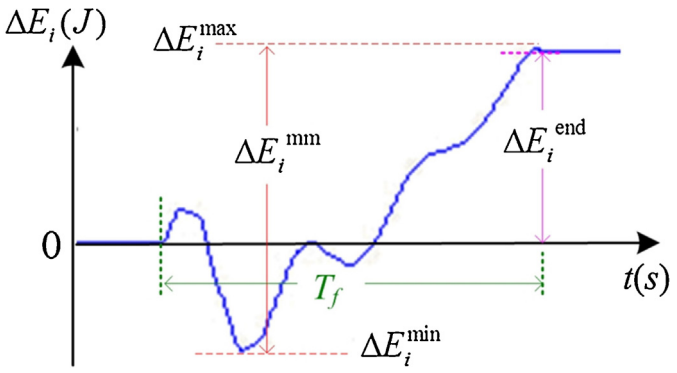

Fig. 3. Characteristic values of ΔE_i.

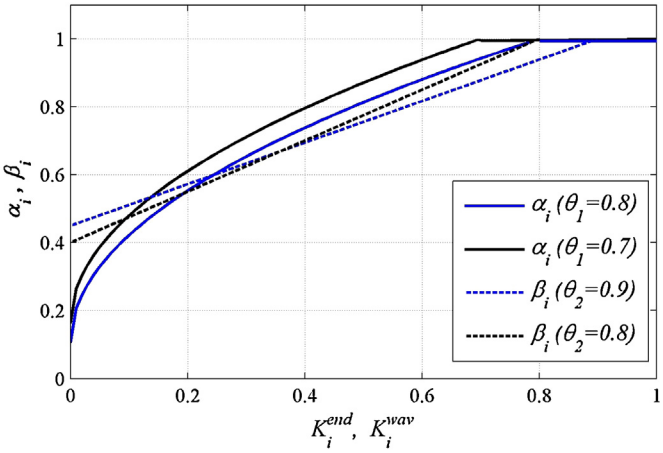

Fig. 4. Distribution characters of coefficients α_i and β_i.

4.1.1. Coefficient of polarity

First, we define $\pi_i = sgn(c_i)$ as the polarity coefficient of c_i. Let ΔE_i^{end} and ΔE_i^{mm} be the final and peak-to-peak values, respectively, as shown in Fig. 3. These two key values describe the characteristics of DE signal during the disturbance event. The value of ΔE_i^{mm} can be obtained by:

$$\Delta E_i^{\mathrm{mm}} = \Delta E_i^{\max} - \Delta E_i^{\min} \tag{5}$$

Then, to indicate the relative direction of the TVDS, the sign function $sgn(\cdot)$ is used to determine the polarity π_i:

$$\pi_i = \begin{cases} \mathrm{sgn}(+\Delta E_i^{end}), & \text{if PQ event is a voltage sag} \\ \mathrm{sgn}(-\Delta E_i^{end}), & \text{if PQ event is a voltage swell} \end{cases} \tag{6}$$

where

$$\mathrm{sgn}(\Delta E_i^{end}) = \begin{cases} +1, & if \quad \Delta E_i^{end} > 0 \\ 0, & if \quad \Delta E_i^{end} = 0 \\ -1, & if \quad \Delta E_i^{end} < 0 \end{cases} \tag{7}$$

4.1.2. Coefficient of disturbance intensity

In the same condition with noise or errors, the credibility of the direction-judgment result should be reduced when the disturbance intensity is relatively weaker [22,23]. In addition to common influence factors of the disturbance intensity, such as disturbance event itself, distance between the TVDS and the PQM, bypass flow, according to the second rule of influence, the DG integration should also be considered in the disturbance intensity.

Therefore, the coefficient α_i of the influence of the disturbance intensity to the reliability of the direction-judgment result is defined as:

$$\alpha_i = \begin{cases} 1, & K_i^{end} > \theta_1 \\ \sqrt{K_i^{end}} + \left(1 - \sqrt{\theta_1}\right), & 0 \le K_i^{end} \le \theta_1 \end{cases} \tag{8}$$

in which

$$K_i^{\mathrm{end}} = \left| \frac{\Delta E_i^{\mathrm{end}}}{\Delta E_{\max}^{\mathrm{end}}} \right| \tag{9}$$

where $\Delta E_{\max}^{end}$ is the maximum among all ΔE_i^{end}, and θ_1 is the threshold value. $\sqrt{(\cdot)}$ is used to prevent α_i from being too small, and the value range of this coefficient is set as $(1 - \sqrt{\theta_1}) \le \alpha_i \le 1$. As shown in Fig. 4, there is a strong positive correlation between α_i and K_i^{end}.

4.1.3. Coefficient of fluctuation characteristic

The fluctuation characteristic of the DE signal is also related to the reliability of the direction-judgment result [14]. If the DE signal fluctuates frequently and fails to keep strict monotonicity, the reliability of the direction-judgment result will be reduced. Therefore, we define the coefficient β_i as:

$$\beta_i = \begin{cases} 1, & K_i^{\mathrm{wav}} > \theta_2 \\ \dfrac{(2-\theta_2)}{2\theta_2} K_i^{\mathrm{wav}} + \dfrac{\theta_2}{2}, & 0 \le K_i^{\mathrm{wav}} \le \theta_2 \end{cases} \tag{10}$$

in which

$$K_i^{\mathrm{wav}} = \left| \frac{\Delta E_i^{end}}{\Delta E_i^{mm}} \right| \tag{11}$$

where K_i^{wav} is a ratio of the fluctuation characteristic of the DE signal, and θ_2 is the threshold value. The value range of this coefficient is $(\theta_2/2) \le \beta_i \le 1$. As shown in Fig. 4, there is also a strong positive correlation between β_i and K_i^{wav}.

With the three coefficients defined above, the monitoring-credibility is defined as:

$$c_i = \pi_i \cdot \alpha_i \cdot \beta_i \tag{12}$$

By definition, c_i is a signed quantitative index ranging from −1.0 to +1.0. Its polarity indicates whether the TVDS is in the down-area or in the up-area of PQM_i, same as in existing methods [11–13]; in addition, its absolute value $|c_i|$ will also indicate the credibility of the direction-judgment result. Combining the values of all monitoring-credibility at each PQM in the NPQMS, a matrix of monitoring-credibility is computed by:

$$C_{m\times 1}^{cre} = \left[c_1, \quad c_2, \quad \ldots, \quad c_m \right]^T \tag{13}$$

4.2. Partial-credibility

To solve the problem of possible direction misjudgment caused by the first rule of influence of the DG integration, a partial credibility c_j^{par} is defined to verify whether there is a TVDS at L_j when F is locating on $Link_{(G\_DG)}$. We define the partial-DE as follows:

$$\Delta E_j^{\mathrm{par}} = \Delta E_j^{\mathrm{end}} - \Delta E_{Lj} - \Sigma \Delta E_j^{\mathrm{out}} \tag{14}$$

where $\sum \Delta E_j^{out}$ is the summation of the DE values of all the outgoing branches connected to the nearest bus in the down-area of L_j, and ΔE_{Lj} is the DE loss at L_j, which can be calculated from the disturbance current ΔI_j. Fig. 5 shows the components of ΔE_1^{par} at

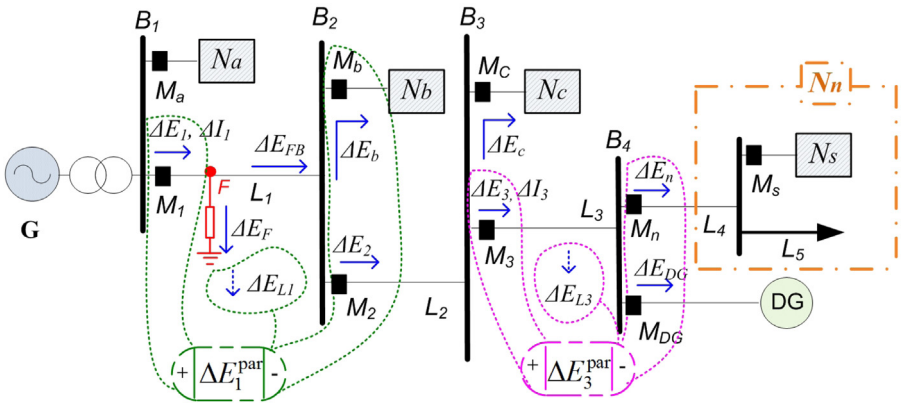

Fig. 5. Characteristic values of partial-DE.

L_1 and ΔE_3^{par} at L_3. The significant difference of the values of ΔE_j^{par} in two different situations is given as:

$$\Delta E_j^{\text{par}} \approx \begin{cases} \Delta E_F^{\text{end}}, & \text{if } F \text{ is at} L_j \\ 0, & \text{if } F \text{ is not at} L_j \end{cases} \tag{15}$$

where ΔE_F^{end} is the final value of the DE signal at F.

We notice that the value of the partial-DE cannot be directly calculated at load branches, such as L_5 in Fig. 5, without a terminal bus. Supposing that the total number of the load branches is δ, the number of ΔE_j^{par} that can be obtained by Eq. (14) is $l-\delta$. To distinguish whether one line is a load branch or not, an identification index μ is defined as:

$$\mu = \frac{1}{l-\delta-1}\left(\sum_{j=1}^{l-\delta} K_j^{\text{par}} - 1\right) \tag{16}$$

in which

$$K_j^{\text{par}} = \left|\frac{\Delta E_j^{\text{par}}}{\Delta E_{\max}^{\text{par}}}\right| \tag{17}$$

where $\Delta E_{\max}^{par}$ is the maximum of all ΔE_j^{par}. The values of K_j^{par} are relatively small in general except for the line of TVDS. The index μ is an adjusted mean of all K_j^{par}, subtracting 1 from the summation of k_j^{par} to keep its value between 0 and 1. It is close to 0 if F is not on a load branch and close to 1 otherwise. Considering the measurement error, the threshold value of μ is set to θ_3, and the partial-credibility corresponding to L_j can be defined as:

$$c_j^{\text{par}} = \begin{cases} +1, & \text{if } \mu \le \theta_3, L_j \in \text{Link}_{(G-\text{DG})} \& K_j^{\text{par}} = 1 \\ -1, & \text{if } \mu \le \theta_3, L_j \in \text{Link}_{(G-\text{DG})} \& K_j^{\text{par}} < 1 \\ 0, & \text{if } \mu > \theta_3 \text{ or } L_j \notin \text{Link}_{(G-\text{DG})} \end{cases} \tag{18}$$

5. TVDS location based on IPSO

5.1. Overall structure of the proposed approach

For integrated utilization of the multi-source information, such as monitoring-credibility of direction-judgment, partial-credibility for DG integration, grid topology, arrangement of PQMs, etc., we employ an IPSO algorithm with well-designed search space and evaluation function to locate the TVDS for DG integrated smart grid [25]. Fig. 6 shows the overall structure of the proposed fault-tolerant approach.

With detailed analysis of the factors including DG integration, disturbance intensity and fluctuation characteristic, the monitoring-credibility and partial-credibility to the direction-judgment results at all PQMs are constructed. Then they are utilized to build the optimal model for TVDS location based on the IPSO, which mainly includes the definitions of matrix-particle and search space, iteration strategy of velocity and position, and evaluation function of fitness.

5.2. Matrix-based particle and search space

As the foundation of the IPSO algorithm, a matrix-particle X_n is constructed for the nth particle in the matrix-particle swarm for all $n \in \{1, \ldots, \tilde{n}\}$, where $\tilde{n}$ is the given size of the particle swarm. As shown in Fig. 7, the whole matrix X_n is used as a particle, whose dimension is the same as the direction-matrix $D_{m\times 1}^{dir}$.

For $i \in \{1, 2, \ldots, m\}$, each element x_{ni} in X_n indicates the direction-judgment result at PQM_i with two possible values (i.e. +1 or −1). Therefore, if we use the general PSO algorithm [26], the possible positions of X_n in the search space will be 2^m. However, in a power grid with certain topology, for $j \in \{1, 2, \ldots, l\}$, one can assume that a disturbance event occurs in sequence on each L_j. By observing the relative positions of each PQM and L_j, we can construct a corresponding expected direction-matrix D_{Lj}^{exp} for each case, according to the element assignment method in Eq. (1). The

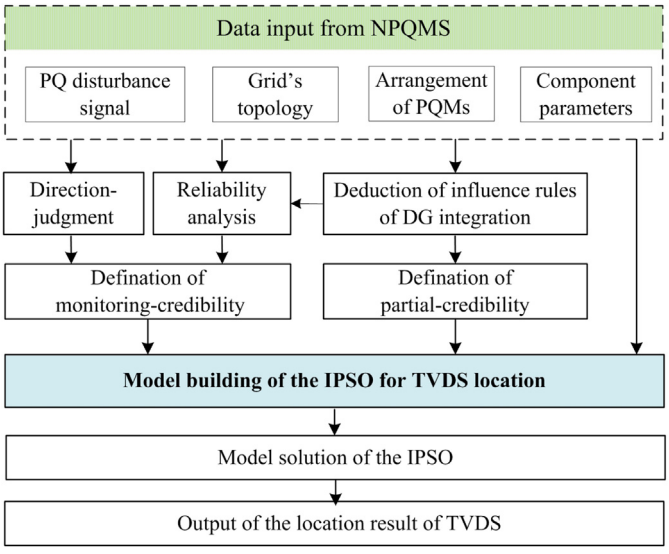

Fig. 6. Overall structure of the proposed approach.

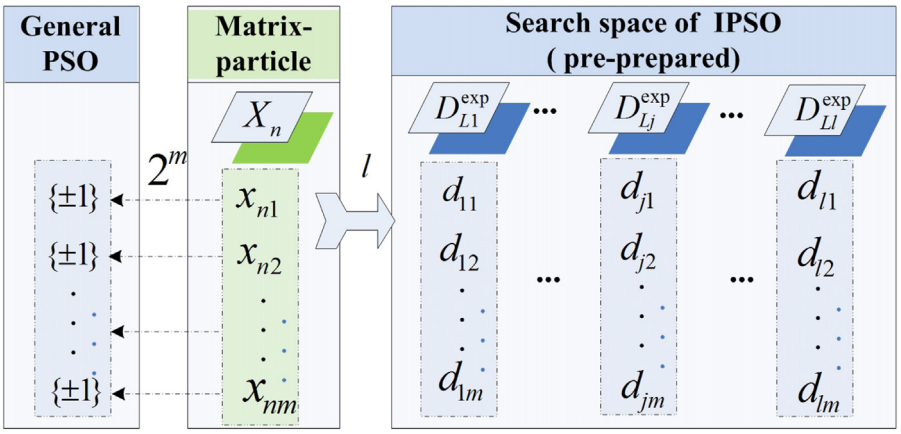

Fig. 7. Structure of the matrix-particle and search space.

total number of $D_{Lj}^{\exp}$ equals to the total number of lines in the grid, and the structure of $D_{Lj}^{\exp}$ is consistent with the direction-matrix $D_{m\times 1}^{dir}$, as shown in Fig. 7.

When an actual disturbance event occurs in the grid, all the potential positions of X_n are in the pre-prepared set $\{D_{Lj}^{\exp}|j = 1, 2, \ldots, l\}$, which is also the search space of X_n. Then the number of possible particle positions in the search space is only l. Therefore, the search space of the proposed IPSO model based on the matrix-particle is reduced greatly from 2^m to l.

5.3. Iteration strategy

The velocity of X_n is v_n, and we define it to be an integer number with the range of $1 \le v_n \le l-1$. The kth iteration of v_n is defined as:

$$v_n^{k+1} = \begin{cases} 1 + \mathrm{int}(\hat{v}_n), & if \quad \mathrm{int}(\hat{v}_n) < l-2 \\ l-1, & if \quad \mathrm{int}(\hat{v}_n) \ge l-2 \end{cases} \tag{19}$$

where

$$\hat{v}_n^{k+1} = \omega v_n^k + \lambda_1 r_1^k \sum_{i=1}^{m} \left| p_{ni}^k - x_{ni}^k \right| + \lambda_2 r_2^k \sum_{i=1}^{m} \left| g_i^k - x_{ni}^k \right| \tag{20}$$

and $\hat{v}_n$ is an intermediate variable, $int(\cdot)$ is the rounding function, ω is an inertia weight, λ_1 and λ_2 are the acceleration factors, r_1 and r_2 are random numbers that take values from 0 to 1, and x_{ni}^k is the element of X_n in the kth iteration. g_i^k and p_{ni}^k are the global optimal position G_{best} and local optimal position $P_{best,n}$ in the kth iteration, respectively.

When $X_n^k = D_{Lj}^{\exp}$, the kth iteration of the nth matrix-particle is defined as:

$$X_n^{k+1} = \begin{cases} D_{L(j+v_n^{k+1})}^{\exp}, & if \quad s_n^{k+1} \ge 0.5 \\ D_{L(j-v_n^{k+1})}^{\exp}, & if \quad s_n^{k+1} < 0.5 \end{cases} \tag{21}$$

where

$$D_{L(j+v)}^{\exp} = \begin{cases} D_{L(j+v-l)}^{\exp}, & if \quad j+v > l \\ D_{L(j+v)}^{\exp}, & if \quad 1 \le j+v \le l \\ D_{L(j+v+l)}^{\exp}, & if \quad j+v < 1 \end{cases} \tag{22}$$

and s_n is a random number in the range of $0 \le s_n \le 1$ to adjust the search direction, and $v = \pm v_n^{k+1}$ is a velocity variable to prevent overflow of the search space.

5.4. Evaluation function

To synthetically utilize the significant information including the monitoring-credibility and the partial-credibility to obtain the accurate result of TVDS location considering the multiple influence factors, the evaluation function is carefully constructed to evaluate the fitness of each X_n. According to Eqs. (13) and (18), the fitness evaluation function with three different cases can be defined as follows:

$$\begin{aligned} F(X_n) &= \left| c_j^{\mathrm{par}} - 1 \right| \cdot \sum_{i=1}^{m} \frac{\left| x_{ni} - \mathrm{sgn}(c_i) \right| \cdot |c_i|}{2} + e_p \cdot \left| c_j^{\mathrm{par}} \cdot (c_j^{\mathrm{par}} - 1) \right| \\ &= \begin{cases} 0, & if c_j^{\mathrm{par}} = +1 \\ \sum_{i=1}^{m} \left| x_{ni} - \mathrm{sgn}(c_i) \right| \cdot |c_i| + 2e_p, & if c_j^{\mathrm{par}} = -1 \\ \sum_{i=1}^{m} \frac{\left| x_{ni} - \mathrm{sgn}(c_i) \right| \cdot |c_i|}{2}, & if c_j^{\mathrm{par}} = 0 \end{cases} \end{aligned} \tag{23}$$

where c_j^{par} is consistent with the current position of the matrix-particle. In this evaluation function, the first term is critical, in which the difference between X_n and $sgn(C_{m\times 1}^{cre})$ along with the value of $|c_i|$ are utilized to evaluate the fitness. The second term is the penalty term, and its coefficient e_p is the penalty factor [27,28]. The partial-credibility c_j^{par} classifies the evaluation function into three possible result options. According to the evaluation value, more credibility support means less difference and better potential solution.

5.5. Procedures of IPSO

Fig. 8 shows the detailed procedures of the IPSO. In the initialization, k^{end} is defined as the maximum iterations, and the initial value of each X_n is randomly chosen from $\{D_{Lj}^{\exp}|j = 1, 2, \ldots, l\}$. The fitness of each X_n is evaluated by using Eq. (23), and all the positions and velocities in the swarm are updated according to Eqs. (19)–(22).

The kth iteration of $P_{best,n}$ is defined as follows:

$$P_{best,n}^{k+1} = \begin{cases} P_{best,n}^k, & if \quad F(P_{best,n}^k) \le F(X_n^{k+1}) \\ X_n^{k+1}, & if \quad F(P_{best,n}^k) > F(X_n^{k+1}) \end{cases} \tag{24}$$

and the optimal one in the set $\{P_{best,n}^k|n = 1, 2, \ldots, \tilde{n}\}$ is assigned to G_{best}^k. In the step of convergence checking, the loop breaks when $F(G_{best}^k) = 0$ or $k = k^{end}$, and the output is G_{best}^k. Finally, we assume

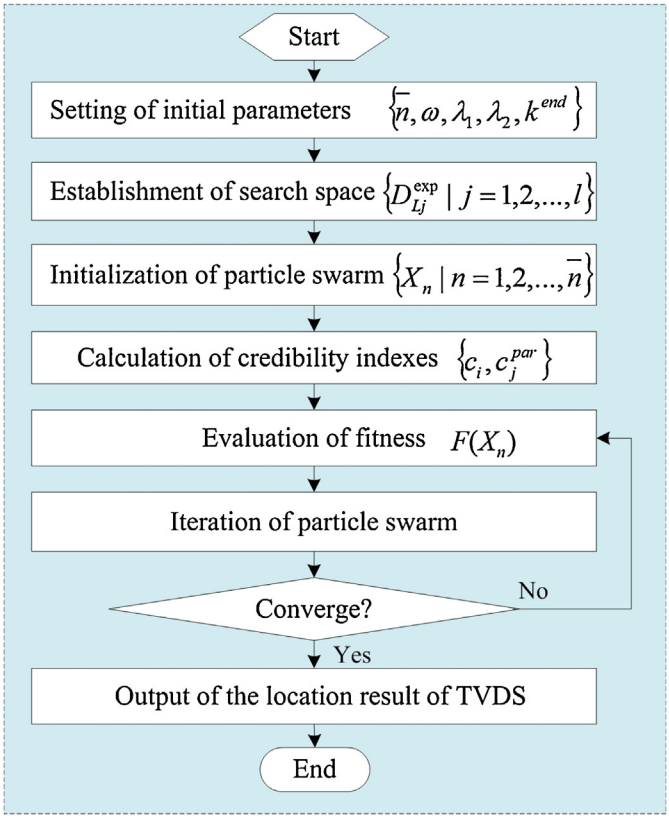

Fig. 8. Flowchart of the IPSO model solution.

Table 1
Numbers of major components.

Bus	Line	Load branch	DG	Actual PQM	Virtual PQM
34	33	25	2	29	31

Table 2
Descriptions of different transient voltage disturbance events.

Event	Event description	L_j
F_1	Three phase L-G fault at Line 830-854.	L_{25}
F_2	Starting of large inductive load at Bus 810.	L_6
F_3	Voltage swell event at Line 858-834.	L_{36}
F_4	Short-time increase of large capacitance at Bus 838.	L_{58}

that the optimal output G_{best}^k is corresponding to D_{Lj}^{exp} in the search space, and L_j is the optimal location of the TVDS.

6. Simulation analysis

6.1. Simulation model description

Simulations were performed on a typical IEEE 34 node test feeder with a nominal voltage of 24.9 kV [29], as shown in Fig. 9. In addition, two DGs are connected to the Bus 820 and 856 to demonstrate the influences of the DG integration. The nominal power of each DG is set as 300 kW. The monitors include both the actual PQMs and the virtual PQMs based on the state estimation. The numbers of the main components of this system are shown in Table 1.

In the following analysis, all the lines and load branches are indexed from L_1 to L_{58}. The monitors are indexed from M_1 to M_{58}, plus two PQMs for the DGs. The applied transient voltage disturbance events, including the causes and the positions, are shown in Table 2. The threshold values in Eqs. (8), (10) and (18) are set as:

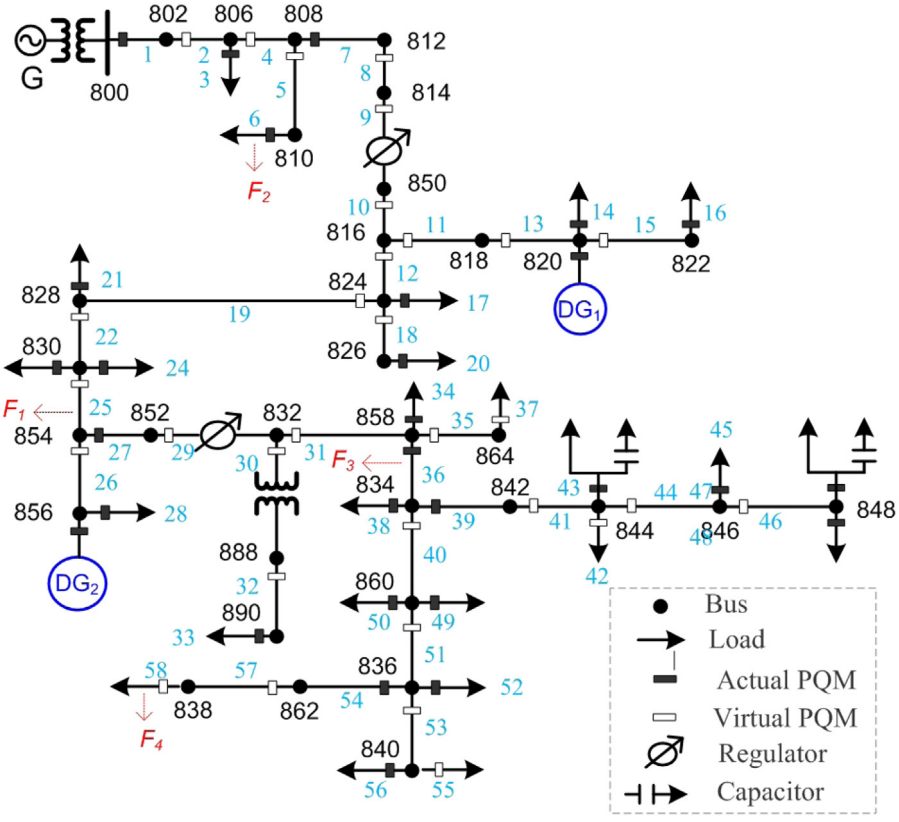

Fig. 9. IEEE 34 node feeder with integrated DGs.

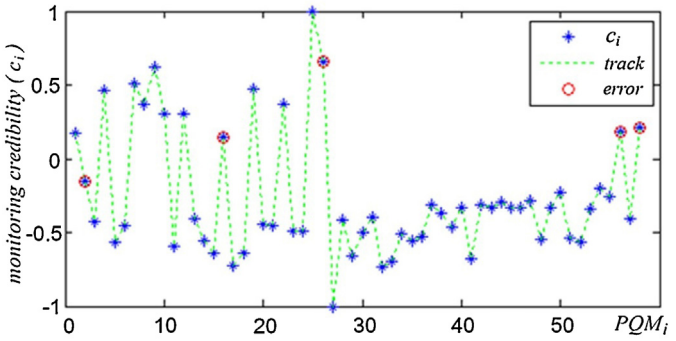

Fig. 10. Monitoring-credibility at each PQM (for event F_1).

$\theta_1 = 0.8$, $\theta_2 = 0.9$, and $\theta_3 = 0.5$. The initial parameters for the IPSO are set as: $\tilde{n} = 5$, $k^{end} = 50$, ω=0.5, and $\lambda_1 = \lambda_2 = 0.25$. In this case $l = 60$, so the coefficient in Eq. (23) is set as: $e_p = \sqrt{l}/2$. Then, the penalty factor is large enough comparing with the order of magnitude of the evaluation function. All the simulations are carried out in the Matlab/Simulink environment.

6.2. Misjudgments and credibility analysis

To simulate the misjudgments caused by the actual interferences, the Gaussian white noise (GWN) is added to the grid when the disturbance events occur. The mean value and variance of the GWN at each PQM are randomly distributed in the range of $[-5\%P_i^{ss}, +5\%P_i^{ss}]$ and $[0, (5\%P_i^{ss})^2]$ respectively, where P_i^{ss} is the steady-state value of the active power at PQM_i.

For the disturbance event F_1, the monitoring-credibility at each PQM is shown in Fig. 10. There are five errors in all the direction-judgment results. The error at L_{26} is caused by the first rule of influence of the DG integration, and the other errors are caused by the weak disturbance signals with strong noise. The comparison of the disturbance characteristics at M_{26} and M_{27} are shown in Fig. 11(a) and (b). Although Line 854-856 and Line 854-852 are at the same node, the direction-judgment results are different. The result at M_{27} is correct, while the misjudgment takes place at M_{26} due to it is on $Link_{(F\_DG_2)}$. This direction misjudgement is caused by the first rule of influence of the DG integration.

In Fig. 11(a) and (b), the intensity of the DE signals at M_{26} and M_{27} are relatively large, so the additional GWN can only change their numerical values slightly but not the polarities. However, monitors distant from F_1 are easier to be affected by the external interferences. Fig. 11(c) and (d) shows the direction misjudgment caused by the GWN at M_{16}. The key coefficients and indexes about the credibilities of direction-judgment at these five misjudgment points are listed in Table 3.

Table 3
Key parameters at misjudgment points of event F_1.

Name	L_2	L_{16}	L_{26}	L_{56}	L_{58}
Expected d_i	+1	−1	−1	−1	−1
π_i	−1	+1	+1	+1	+1
K_i^{end}	0.005	0.003	0.282	0.015	0.019
α_i	0.170	0.154	0.631	0.222	0.214
K_i^{wav}	0.878	0.984	0.991	0.392	0.741
β_i	0.987	1.0	1.0	0.717	0.911
c_i	−0.168	+0.154	+0.631	+0.159	+0.217
K_j^{par}	0.042	Null	0.027	Null	Null
c_j^{par}	−1	0	−1	0	0

6.3. IPSO analysis

Taking the event F_1 for example, the convergence properties of each X_n in the search process are shown in Fig. 12(a). Most of the matrix-particles quickly converged to quite small fitness values; particularly, X_1 only needs 13 iterations to reach the global optimum (i.e. zero solution). Some abrupt points in the fitness curves

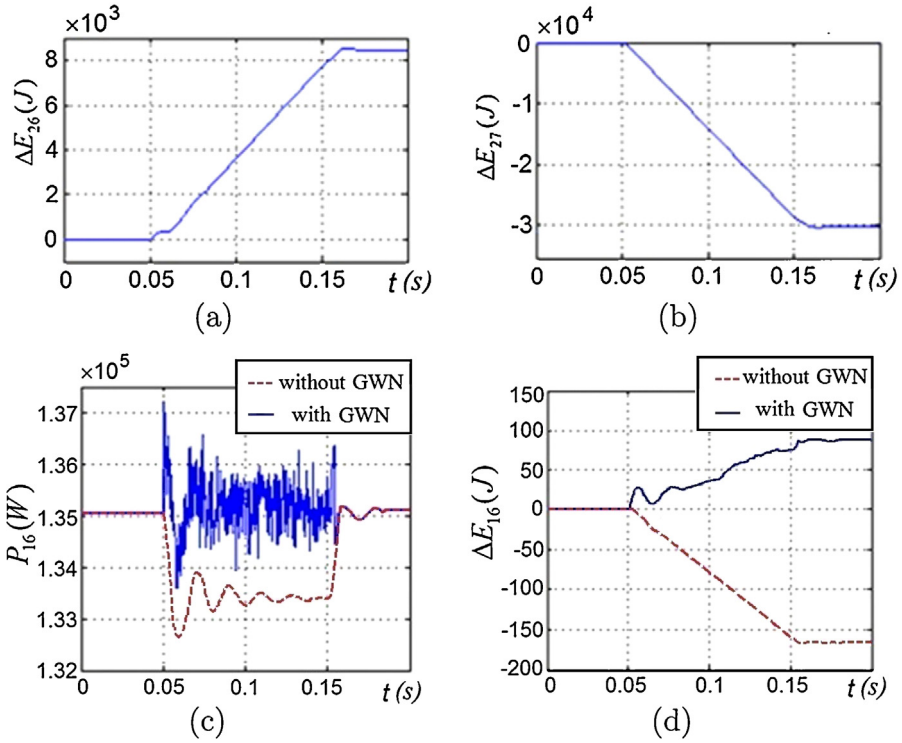

Fig. 11. Misjudgments caused by the DG integration and the noise: (a) DE signal at M_{26}; (b) DE signal at M_{27}; (c) comparison of the power signals at M_{16}; (d) comparison of DE signals at M_{16}.

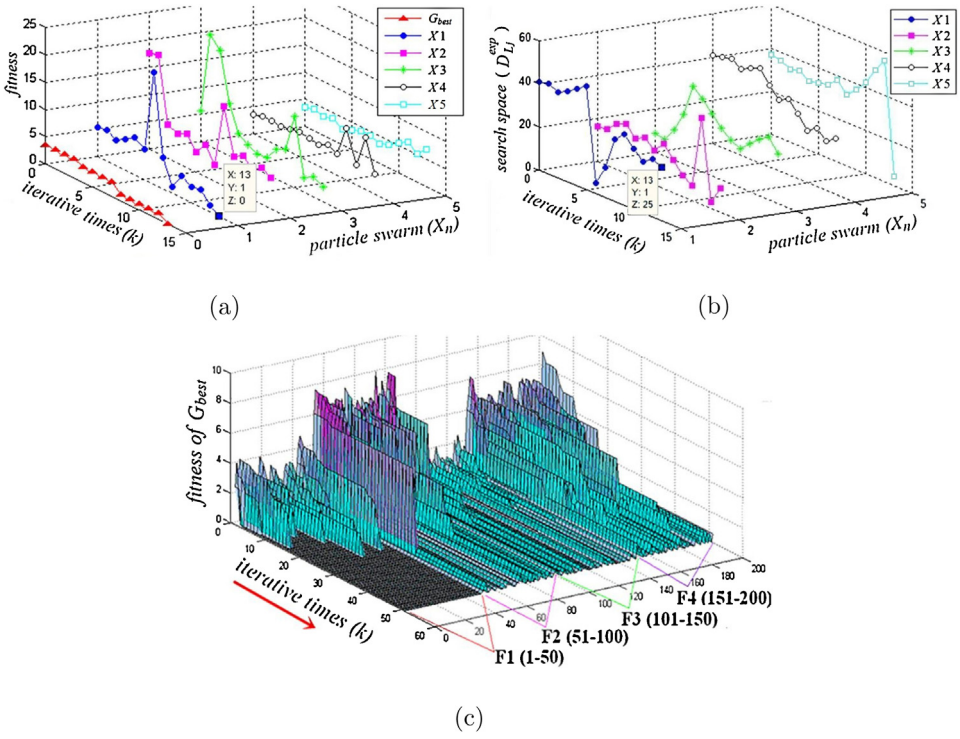

Fig. 12. Process analysis of the IPSO. (a) Convergence of fitness for F_1. (b) Search paths of each matrix-particle for F_1. (c) Convergence of G_{best} for all the events.

of X_n are caused by the modification of the value of c_j^{par} from the DG integration.

Fig. 12(b) shows the search paths of each matrix-particle, and the values on the vertical dimension show their positions in the available search space in each search iteration. Corresponding to the zero solution in X_1, we found $G_{best}^{13} = D_{L25}^{exp}$, which means the optimal output in the whole search process is L_{25}. It is consistent with the location of the given disturbance event F_1.

For each kind of the disturbance events listed in Table 2, 50 groups of disturbance data are obtained by simulating 50 cases with random intensities of noise interferences. The convergence of the proposed IPSO for these 200 tests (i.e. the global optimal G_{best}) are shown in Fig. 12(c). The overall convergence speed of the proposed approach is fairly fast.

6.4. Performance comparison

6.4.1. Comparison in the second category of research methodologies

Considering different intensities of noise interference, the 200 tests are divided into four groups according to the number of direction misjudgments. Using these four groups, we compare the fault tolerance of the proposed IPSO approach with the traditional matrix (TM) algorithm [12,13] and the improved matrix algorithm with disturbance measure (DM) [22]. The results are shown in Table 4. All algorithms have successful identified the TVDS location in the 28 misjudgment-free tests. Among the 172 tests with direction misjudgments, the DM algorithm located the TVDS correctly in 107 of them, while the TM algorithm failed to locate any correctly due to its fault-intolerance. Meanwhile, there were only seven mistakes made by the proposed IPSO approach. In summary, the TM algorithm only works well with the absolute reliability of all direction-judgment results in the whole NPQMS; the DM algorithm's performance is not as competitive as the proposed method, because it fails to consider the influence of DG integration and other factors; the proposed IPSO approach provided a remarkable improvement with fault-tolerant capability.

According to above analysis, the performances of both the TM and the DM algorithms are far from satisfactory when direction misjudgments occur in the NPQMS, which are according with their work mechanisms. In contrast, the major cause of the remarkable performance of the IPSO approach proposed in this paper is taking into full account of the influence factors of direction judgment, the credibility indexes, and the comprehensive utilization of multi-source information. However, due to the cumulative effect of multiple direction misjudgments in some occasional cases, even if sufficient consideration of the DG integration and other influence factors, it is still hard to guarantee the absolutely correctness of the location result.

6.4.2. Comparison with the first category of research methodologies

The first category of research methodologies for TVDS location are based primarily on pattern recognition and intelligent classifiers such as artificial neural networks (ANN) [7,8], self-organizing map (SOM) [6], decision-tree (DT) [9], etc. The comparison shows that these methods are satisfying in accuracy and cost performance under the conditions of smaller network scope, fixed topology and definitive type of transient voltage disturbance event induced by same one cause. While for the smart grid where the NPQMS is available, the proposed IPSO method has more advantages

Table 4
Fault tolerance of three location approaches in the second category.

Misjudgments	Test times	TM		DM		Proposed IPSO	
		Correct	%	Correct	%	Correct	%
0	28	28	100	28	100	28	100
1 ~ 3	91	N/A	–	64	70.3	89	97.8
4 ~ 5	37	N/A	–	22	59.5	35	94.6
≥6	44	N/A	–	21	47.7	41	93.2
Total	200	28	14.0	135	67.5	193	96.5

in applicability, accuracy, especially in the scenarios where the topology and power flow change frequently in large-scale smart grids with DGs integration. Moreover, the remarkable performance in real-time makes it promising for fast TVDS location.

7. Conclusion

In this paper, we proposed a new fault-tolerant IPSO approach to locate the TVDS in the DG integrated smart distribution grid. Specifically, two rules of influence of the DG integration on the direction-judgment were first presented under different scenarios. The monitoring-credibility and partial-credibility were then defined to describe the reliability of the direction-judgment result and correct potential misjudgment caused by the DG integration, respectively. Then, an improved PSO was proposed to synthetically utilize the multi-source information and make the decision-making. Simulation results on the IEEE 34 node test feeder validated the effectiveness of the proposed approach. Compared with the existing matrix-based methods, the proposed approach has shown advantages of high accuracy, fault-tolerance capability, applicability and fast convergence for smart distribution grids with DG integration.

There are two future research directions based on the work in this paper. One direction is the effective verification of the correctness of the TVDS location under various conditions in actual application systems. The other is that, considering the influence of the DG integration, more comparisons should be carried out with the first category of research methodologies for TVDS location.

Acknowledgments

The research was supported by the Natural Science Foundation of China (Grant Nos. 51507153, 51207139), Zhejiang Provincial Natural Science Foundation of China (Grant No. LY17E070005), and the China Scholarship Council (Grant No. 201408330220).

References

[1] S.-H. Jo, S. Son, J.-W. Park, On improving distortion power quality index in distributed power grids, IEEE Trans. Smart Grid 4 (1) (2013) 586–595.
[2] D.D. Ferreira, J.M. de Seixas, A.S. Cerqueira, A method based on independent component analysis for single and multiple power quality disturbance classification, Electric Power Syst. Res. 119 (2015) 425–431.
[3] Z. Liu, Y. Cui, W. Li, A classification method for complex power quality disturbances using EEMD and rank wavelet SVM, IEEE Trans. Smart Grid 6 (4) (2015) 1678–1685.
[4] O. Ozgonenel, T. Yalcin, I. Guney, U. Kurt, A new classification for power quality events in distribution systems, Electric Power Syst. Res. 95 (2013) 192–199.
[5] R.H.G. Tan, V.K. Ramachandaramurthy, Voltage sag acceptability assessment using multiple magnitude-duration function, IEEE Trans. Power Deliv. 27 (4) (2012) 1984–1990.
[6] E. Bentley, G. Putrus, S. McDonald, P. Minns, Power quality disturbance source identification using self-organising maps, Gener. Transm. Distrib. IET 4 (10) (2010) 1188–1196.
[7] A. Abu-Elanien, M. Salama, A wavelet-ANN technique for locating switched capacitors in distribution systems, IEEE Trans. Power Deliv. 24 (1) (2009) 400–409.
[8] Y.-Y. Hong, B.-Y. Chen, Locating switched capacitor using wavelet transform and hybrid principal component analysis network, IEEE Trans. Power Deliv. 22 (2) (2007) 1145–1152.
[9] Y. Dong, C. Zheng, M. Kezunovic, Enhancing accuracy while reducing computation complexity for voltage-sag-based distribution fault location, IEEE Trans. Power Deliv. 28 (2) (2013) 1202–1212.
[10] T. Demirci, A. Kalaycioglu, D. Kucuk, O. Salor, M. Guderl, S. Pakhuylu, T. Atalik, T. Inan, I. Cadirci, Y. Akkaya, S. Bilgen, M. Ermis, Nationwide real-time monitoring system for electrical quantities and power quality of the electricity transmission system, Gener. Transm. Distrib. IET 5 (5) (2011) 540–550.
[11] I.-Y. Chung, D.-J. Won, J.-M. Kim, S.-J. Ahn, S.-I. Moon, Development of a network-based power quality diagnosis system, Electric Power Syst. Res. 77 (8) (2007) 1086–1094.
[12] D.-J. Won, I.-Y. Chung, J.-M. Kim, S.-I. Moon, J.-C. Seo, J.-W. Choe, A new algorithm to locate power-quality event source with improved realization of distributed monitoring scheme, IEEE Trans. Power Deliv. 21 (3) (2006) 1641–1647.
[13] G. Weng, Y. Zhang, H. He, A novel location algorithm for power quality disturbance source using chain table and matrix operation, Int. Rev. Electr. Eng. 6 (6) (2011) 2746–2753.
[14] A. Parsons, W. Grady, E. Powers, J. Soward, A direction finder for power quality disturbances based upon disturbance power and energy, IEEE Trans. Power Deliv. 15 (3) (2000) 1081–1086.
[15] W. Kong, X. Dong, Z. Chen, Voltage sag source location based on instantaneous energy detection, Electric Power Syst. Res. 78 (11) (2008) 1889–1898.
[16] W. Zhang, C. Wang, Transient disturbances location based on improved disturbance power and energy, Autom. Electric Power Syst. 31 (8) (2007) 32–35.
[17] S. Ali, K. Wu, K. Weston, D. Marinakis, A machine learning approach to meter placement for power quality estimation in smart grid, IEEE Trans. Smart Grid 7 (3) (2016) 1552–1561.
[18] A. Farzanehrafat, N. Watson, Power quality state estimator for smart distribution grids, IEEE Trans. Power Syst. 28 (3) (2013) 2183–2191.
[19] N. Woolley, M. Avendao-Mora, A. Woolley, R. Preece, J. Milanovic, Probabilistic estimation of voltage sags using erroneous measurement information, Electric Power Syst. Res. 106 (2014) 142–150.
[20] E.N. Silva, A.B. Rodrigues, M. da Guia da Silva, Stochastic assessment of the impact of photovoltaic distributed generation on the power quality indices of distribution networks, Electric Power Syst. Res. 135 (2016) 59–67.
[21] P.C. Chen, V. Malbasa, Y. Dong, M. Kezunovic, Sensitivity analysis of voltage sag based fault location with distributed generation, IEEE Trans. Smart Grid 6 (4) (2015) 2098–2106.
[22] Q. Guo, Q. Jia, Z. Bo, Locating power-quality event source through disturbance measures, in: 2010 45th International Universities Power Engineering Conference (UPEC), 2010, pp. 1–5.
[23] H. Dong, Q. Guo, Q. Jia, Z. Bo, S. Wang, X. Yang, An algorithm to locate power-quality disturbance source based on disturbance measures and information fusion theory, in: 2011 4th International Conference on Electric Utility Deregulation and Restructuring and Power Technologies (DRPT), 2011, pp. 589–595.
[24] F. Huang, G. Weng, Q. Wang, Location of power quality disturbance source in distribution network with distributed generators, Autom. Electric Power Syst. 39 (9) (2015) 150–155.
[25] H. Renaudineau, F. Donatantonio, J. Fontchastagner, G. Petrone, G. Spagnuolo, J.-P. Martin, S. Pierfederici, A PSO-based global MPPT technique for distributed PV power generation, IEEE Trans. Ind. Electron. 62 (2) (2015) 1047–1058.
[26] P. Li, D. Xu, Z. Zhou, W. Lee, B. Zhao, Stochastic optimal operation of microgrid based on chaotic binary particle swarm optimization, IEEE Trans. Smart Grid 7 (1) (2016) 66–73.
[27] J.J. Jamian, M.N. Muhtazaruddin, M.A. Baharudin, Penalty factor-based optimization algorithm for distributed generation sizing in distribution network, Turk. J. Electr. Eng. Comput. Sci. 24 (3) (2016) 1815–1825.
[28] Z. Zhang, G. Gao, Y. Shi, Credit risk evaluation using multi-criteria optimization classifier with kernel, fuzzification and penalty factors, Eur. J. Oper. Res. 237 (1) (2014) 335–348.
[29] IEEE PES Distribution System Analysis Subcommittee's Distribution Test Feeder Working Group, Distribution Test Feeders, 2010 http://ewh.ieee.org/soc/pes/dsacom/testfeeders/ (accessed 17.09.10).